N95-27355

RTE—A COMPUTER CODE FOR ROCKET THERMAL EVALUATION

Mohammad H.N. Naraghi
Department of Mechanical Engineering
Manhattan College
Riverdale, New York

SUMMARY

The numerical model for a rocket thermal analysis code (RTE) is discussed. RTE is a comprehensive thermal analysis code for thermal analysis of regeneratively cooled rocket engines. The input to the code consists of the composition of fuel/oxidant mixture and flow rates, chamber pressure, coolant temperature and pressure, dimensions of the engine, materials and the number of nodes in different parts of the engine. The code allows for temperature variation in axial, radial and circumferential directions. By implementing an iterative scheme, it provides nodal temperature distribution, rates of heat transfer, hot gas and coolant thermal and transport properties. The fuel/oxidant mixture ratio can be varied along the thrust chamber. This feature allows the user to incorporate a non-equilibrium model or an energy release model for the hot-gas-side. The user has the option of bypassing the hot-gas-side calculations and directly inputting the gas-side fluxes. This feature is used to link RTE to a boundary layer module for the hot-gas-side heat flux calculations.

INTRODUCTION

Thermal analysis is an essential and integral part in the design of rocket engines. The need for thermal analysis is especially important in the reusable engines where an effective and efficient cooling system becomes a crucial factor in extending the engine life. In the new high pressure engines, such as chemical transfer vehicle engines, hot-gas temperature is very high (can reach 7000R at the throat). It is therefore essential to be able to estimate the wall temperature and ensure that the material can withstand such high temperature. Furthermore, an accurate thermal model enables an engine designer to modify the cooling channel configuration for the maximum cooling at high temperature areas.

The thermal phenomena in rocket engines involve interactions among a number of processes. including, combustion in the thrust chamber, expansion of hot-gases through the nozzle, heat transfer from hot-gases to the nozzle wall via convection and radiation, conduction in the wall, and convection to the cooling channel. Further complexities of the thermal analysis in rocket engines are due to three-dimensional geometry, coolant and hot gas heat transfer coefficient dependence on the pressure and wall temperature, unknown coolant pressure drop and properties, axial conduction of heat within the wall, and radiative heat transfer between gases and surfaces of the engine. A comprehensive thermal model must account for all of these items.

RTE [1] is a comprehensive rocket thermal analysis code that uses a number of existing codes and allows interaction among them via some iterative procedures. The code is based on the geometry of a typical regeneratively-cooled engine similar to that shown in Figure 1. It uses CET (Chemical Equilibrium with Transport Properties) [2] and GASP [3] for the

evaluation of hot-gas and coolant properties. The inputs to this code consist of the composition of fuel/oxidant mixtures and flow rates, chamber pressure. coolant entrance temperature and pressure, dimensions of the engine and materials in different parts of the engine, as well as the mesh generation data. This program allows temperature variations in axial, radial and circumferential directions, and by implementing an iterative scheme it provides temperature distributions, rates of heat transfer, and hot-gas and coolant thermal and transport properties. The fuel/oxidant mixture ratio can be varied along the thrust chamber. This feature allows the user to incorporate a nonequilibrium model or an energy release model for the hot-gas-side. The mixture ratio along the thrust chamber is calculated using ROCCID [4] (ROCket Combustor Interactive Design and Analysis Computer Program). ROCCID has been modified to take RTE input and make the mixture ratio variable along the thrust chamber. The user has the option of bypassing the hot-gas-side calculations and directly inputting gas side fluxes. This feature is used to link RTE to a boundary layer program for the hot-gas-side heat flux calculation. The procedure for linking RTE to a hot-gas side program. TDK [5] (Two-Dimensional Kinetics Nozzle Performance Computer Program) is described here.

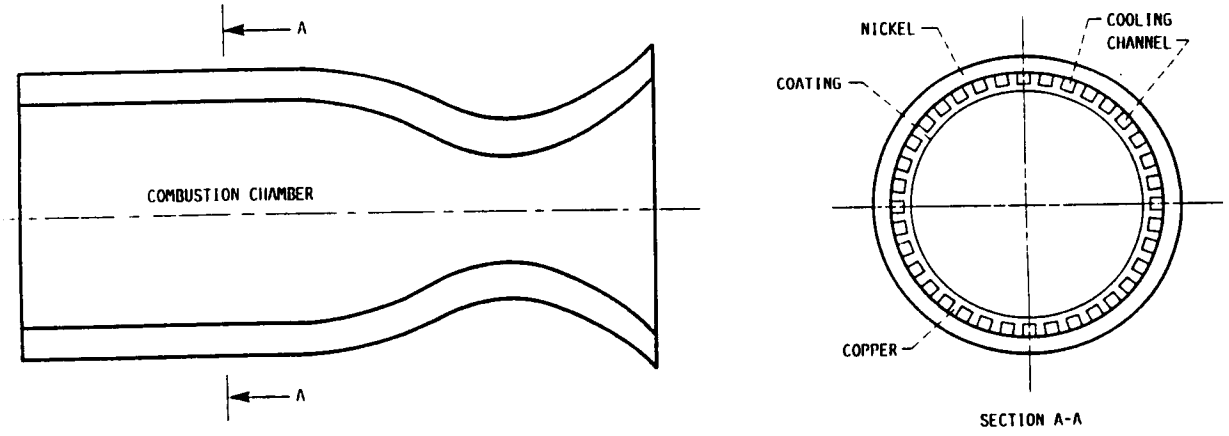

Figure 1. A Rocket Thrust Chamber and Nozzle

NUMERICAL MODEL

The numerical model of the RTE is based on the geometry of a typical regeneratively-cooled thrust chamber (shown in Figure 1). The wall can consist of three layers: a coating, the channel, and the closeout. These three layers can be different materials or the same material. The number of cooling channels in the wall are also specified by the user. For the numerical procedure, the rocket thrust chamber and nozzle are subdivided into a number of stations along the longitudinal direction, as shown in Figure 2. The thermodynamic and transport properties of the combustion gases are evaluated using the chemical equilibrium composition computer program developed by Gordon and McBride [2, 6] (CET, Chemical Equilibrium with Transport properties). The GASP (GAS Properties) [3] or WASP (Water And Steam Properties) [7] programs are implemented to obtain coolant thermodynamic and transport properties. Since the heat transfer coefficients of the hot-gas and coolant sides are related to

surface temperatures, an iterative procedure is used to evaluate heat transfer coefficients and adiabatic wall temperatures.

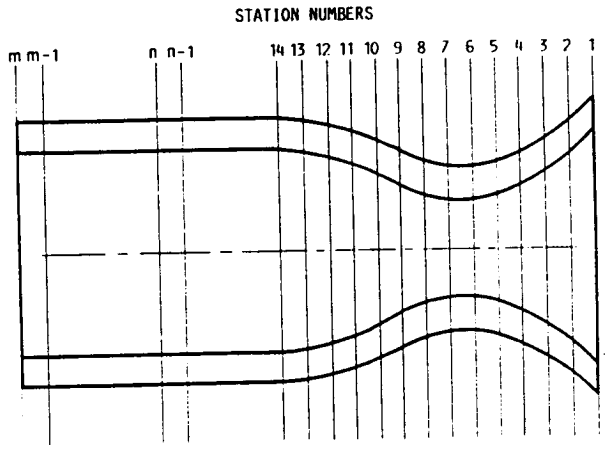

Figure 2. A Rocket Thrust Chamber Subdivided into a Number of Stations

The temperature distribution within the wall is determined via a three-dimensional finite difference scheme. In this method, finite difference grids are superimposed throughout the wall at different stations. The temperature of each node is then written in terms of temperatures of neighboring nodes (the four closest nodes at the same station and two nodes at the neighboring stations). The program marches axially from one station to another. At each station the Gauss-Siedel iterative method is used to obtain convergence for the temperature distribution along the radial and circumferential directions. When the axial march is completed, comparison is made between the results of the present march and that of the previous one to see if the convergence criteria in the axial direction has been met. If it is not met, the code starts again at the first station and makes another axial march. The process continues until convergence is achieved. A detailed description of this numerical model is outlined below.

First, the static pressures, temperatures, enthalpies and Mach numbers for the combustion gases are evaluated using the ROCKET subroutine from [2]. It should be noted that these properties are independent of wall temperature and only depend on the cross-sectional area of the nozzle, the propellant used and chamber pressure. Indeed, the heat transfer from hot gases to the chamber and nozzle wall will cause very little change in the gas temperature (the thermodynamic process dominates the transport process).

On the coolant side, the stagnation enthalpy and density at the entrance to the cooling channel are evaluated as functions of the coolant stagnation pressure and temperature ($i_{C0} = i_{C0}(P_{C0}, T_{C0})$ and $\rho_{C0} = \rho_{C0}(P_{C0}, T_{C0})$) using the GASP or WASP programs.

The model now begins its axial marches (passes) starting from the first station. At the first axial march an initial guess for the wall temperature distribution is made. For the next march, however, the results of temperature distribution for the previous march can be used as an initial guess. The hot gas and coolant adiabatic wall temperatures and wall properties can be evaluated at a given station based on the assumed wall temperature distribution using the properties computer codes [2, 6, 3, 7] for the combustion gases and the coolant. The reference enthalpy of the gas side, i_{GX_n} is given by [8]

$$i_{GX_n} = 0.5(i_{GW_n} + i_{GS_n}) + 0.180(i_{G0_n} - i_{GS_n}) \quad (1)$$

where i_{GW_n} is a function of gas static pressure P_{GS_n} and gas-side wall temperature T_{GW_n} and is evaluated using the program given in [2]. The gas-side adiabatic wall enthalpy, i_{GAW_n} is calculated using the following equation [8, 9]

$$i_{GAW_n} = i_{GS_n} + (Pr_{GX_n})^{1/3}(i_{G0_n} - i_{GS_n}) \quad (2)$$

where the gas reference Prandtl number Pr_{GX_n} is

$$Pr_{GX_n} = \frac{C_{pGX_n}\mu_{GX_n}}{k_{GX_n}} \quad (3)$$

C_{pGX_n}, μ_{GX_n} and k_{GX_n} are functions of P_{GS_n} and i_{GX_n}. Once the gas-side adiabatic wall temperature is determined, the wall adiabatic temperature is calculated via

$$T_{GAW_n} = f(P_{GS_n}, i_{GAW_n}) \quad (4)$$

and using the combustion codes [2, 6]. The hot-gas side heat transfer coefficient, h_{G_n} is given by [8]

$$h_{G_n} = \frac{C_{G_n}k_{GX_n}}{d_{G_n}} Re_{GX_n}^{0.8} Pr_{GX_n}^{0.3} \quad (5)$$

where C_{G_n} is the gas-side correlation coefficient given as input and the Reynolds number is defined by

$$Re_{GX_n} = \frac{4W_G}{\pi d_{G_n}\mu_{GX_n}} \frac{T_{GS_n}}{T_{GX_n}} \quad (6)$$

$$T_{GX_n} = f(P_{GS_n}, i_{GX_n}) \quad (7)$$

$$T_{GS_n} = f(P_{GS_n}, i_{GS_n}) \quad (8)$$

Once the hot-gas-side heat transfer coefficient is determined the wall heat flux can be evaluated via

$$q_n = h_{G_n}(T_{GAW_n} - T_{GW_n}) \quad (9)$$

or

$$q_n = \frac{h_{G_n}}{C_{pGX_n}}(i_{GAW_n} - i_{GW_n}) \quad (10)$$

The adiabatic wall temperature and gas-side heat transfer coefficient, calculated from equations (4) and (5), or wall heat flux calculated using equations (9) and (10) will be used in the conduction module to evaluate a revised wall temperature distribution. It should be noted that the formulation given by equations (5-10) yields an approximate value for the wall heat flux. To obtain a more accurate value for the wall heat flux a boundary layer model should be implemented. The procedure for interfacing a boundary layer module to the present model will be described later. Next, attention will be focused on calculating the coolant-side properties and heat transfer coefficient.

For the first station the coolant stagnation enthalpy, static pressure and static density are set equal to the stagnation enthalpy, pressure, and density at the entrance to the cooling channel (i.e., $i_{C0_1} = i_{C0}$, $P_{CS_1} = P_{C0}$ and $\rho_{CS_1} = \rho_{C0}$). For the other stations, the coolant stagnation enthalpy is calculated via

$$i_{C0_n} = i_{C0_{n-1}} + \frac{(q_n^{j-1} + q_{n-1})\Delta S_{n-1,n}}{2W_C} \tag{11}$$

where $\Delta S_{n-1,n}$ is the distance between two neighboring stations $n-1$ and n and q_n^{j-1} is the heat transferred per unit length of the cooling channel from the hot gases to the coolant at station n (calculated from the conduction subroutine at iteration $j-1$). For the first iteration at station n, q_n^{j-1} in equation (11) is not known; therefore the following equation is used to evaluate the stagnation enthalpy

$$i_{C0_n} = i_{C0_{n-1}} + \frac{q_{n-1}\Delta S_{n-1,n}}{W_C} \tag{12}$$

Note that q_{n-1} in equations (11) and (12) are the heat transfer per unit length of cooling channel at the previous station.

The coolant velocity is calculated from the following equation:

$$V_{CS_n} = \frac{W_C}{\rho_{CS_n} A_{C_n} N_n} \tag{13}$$

Note that ρ_{CS_n}, is set equal to ρ_{CO_n} for the first station, and for the other stations is evaluated using the GASP or WASP programs [3, 7] based on the static pressure and enthalpy at the previous iteration, i.e.,

$$\rho_{CS_n}^j = \rho(P_{CS_n}^{j-1}, i_{CS_n}^{j-1}) \tag{14}$$

At the first iteration, however, it is set equal to the static density of the previous station ($\rho_{CS_n}^1 = \rho_{CS_{n-1}}$).

Once the coolant velocity is determined, the static enthalpy can be calculated using the following equation:

$$i_{CS_n} = i_{C0_n} - \frac{V_{CS_n}^2}{2g_c J} \tag{15}$$

The coolant static and reference Reynolds numbers, respectively, are given by:

$$Re_{CS_n} = \frac{W_C d_{C_n}}{A_{C_n} N_n \mu_{CS_n}} \tag{16}$$

and

$$Re_{CX_n} = Re_{CS_n}\left(\frac{\rho_{CW_n}}{\rho_{CS_n}}\right)\left(\frac{\mu_{CS_n}}{\mu_{CW_n}}\right) \tag{17}$$

where μ_{CS_n} is a function of P_{CS_n} and i_{CS_n} and is calculated using the GASP program [3], or the WASP program [7] if the coolant is water. Note also that d_{C_n} is the coolant hydraulic diameter at station n. To employ a better value for the Reynolds number, an average Reynolds number between the entrance and exit to each station is evaluated, i.e.,

$$Re_{CS_{Avg.}} = 0.5(Re_{CS_n} + Re_{CS_{n-1}}) \tag{18}$$

$$Re_{CX_{Avg.}} = 0.5(Re_{CX_n} + Re_{CX_{n-1}}) \tag{19}$$

The Reynolds number in the cooling channel is within the turbulent flow range; hence, the Colebrook equation [10] is used to calculate the friction factor. This equation is given by:

$$\frac{1}{\sqrt{f}} = -2.0 \log \left(\frac{e}{3.7065D} + \frac{2.5226}{Re_{CX_{Avg.}}\sqrt{f}} \right) \tag{20}$$

This implicit equation has been shown to be very closely approximated by the explicit formula [11]

$$\frac{1}{\sqrt{f}} = -2.0 \log \left[\frac{e}{3.7065D} - \frac{5.0452}{Re_{CX_{Avg.}}} \log \left(\frac{1}{2.8257} \left(\frac{e}{D} \right)^{1.1098} + \frac{5.8506}{Re_{CX_{Avg.}}^{0.8981}} \right) \right] \tag{21}$$

The correlation given by equation (21) is only valid for straight channels. To include the curvature effect, the friction factor obtained from equation (21) must be multiplied by the curvature factor given by Itō's correlation [12]:

$$\phi_{Cur.} = \left[Re_{CX_{Avg.}} \left(\frac{r_{C_n}}{R_{Cur._n}} \right)^2 \right]^{1/20} \tag{22}$$

where r_{C_n} is the hydraulic radius of cooling channel, $R_{Cur._n}$ is the radius of curvature. The curvature factor given by equation (22) is valid when $Re_{CX_{Avg.}}(\frac{r_{C_n}}{R_{Cur._n}})^2 > 6$, otherwise, $\phi_{Cur.} = 1$.

Once the friction factors are determined, the viscous pressure drop between stations $n-1$ and n is calculated using Darcy's law [13] which is given by:

$$(\Delta P_{CS_{n-1,n}})_f = \frac{f_n}{8g_c} \left(\frac{\rho_{CS_n} + \rho_{CS_{n-1}}}{d_{C_n} + d_{C_{n-1}}} \right) (V_{CS_n} + V_{CS_{n-1}})^2 \Delta S_{n-1,n} \tag{23}$$

and the momentum pressure drop is calculated via

$$(\Delta P_{CS_{n-1,n}})_M = \left(\frac{2}{(NA_C)_{n-1} + (NA_C)_n} \right) \frac{W_C^2}{g_c} \left(\frac{1}{(\rho_{CS} A_C N)_n} - \frac{1}{(\rho_{CS} A_C N)_{n-1}} \right) \tag{24}$$

An average value of variables between stations n and $n-1$ are used to improve the accuracy. The static pressure at each station is calculated based on the viscous and momentum pressure drops and is given by:

$$P_{CS_n} = P_{CS_{n-1}} - \left[(\Delta P_{CS_{n-1,n}})_f + (\Delta P_{CS_{n-1,n}})_M \right] \tag{25}$$

Once the coolant static pressure is determined, the coolant wall properties which are functions of the static coolant pressure P_{CS_n} and wall temperature, i.e.,

$$C_{p_{CW_n}}, \mu_{CW_n}, k_{CW_n}, i_{CW_n} = f(P_{CS_n}, T_{CW_n}) \tag{26}$$

are evaluated using the GASP or WASP programs. It should be noted that the wall temperature is not constant at a given station; hence, three coolant wall properties which are based on the lower, upper and side wall temperatures are determined. The reference and adiabatic wall enthalpies at the station are, respectively, calculated from the following equations [8]

$$i_{CX_n} = 0.5(i_{CS_n} + i_{CW_n}) + 0.194(i_{C0_n} - i_{CS_n}) \tag{27}$$

and

$$i_{CAW_n} = i_{CS_n} + (Pr_{CX})^{1/3}(i_{C0_n} - i_{CS_n}) \tag{28}$$

The adiabatic wall temperature is a function of the coolant static pressure and the adiabatic wall enthalpy and is evaluated using the GASP program [3]. Note that the Prandtl number in equation (26) is expressed by:

$$Pr_{CX} = \frac{C_{pCX}\mu_{CX}}{k_{CX}} \tag{29}$$

where

$$C_{pCX},\ \mu_{CX},\ k_{CX} = f(P_{CS}, i_{CX})$$

Three correlations may be used to evaluate the heat transfer coefficients in the cooling channels. The simplest one is given by the following correlation (see [8, 9]):

$$Nu = C_{C_n} Re_{CX}^{0.8} Pr_{CX}^{0.4} \tag{30}$$

Most recently, a new correlation is presented in [14, 15]. In this correlation the Nusselt number is given by:

$$\frac{Nu}{Nu_r} = C_{C_n} Re^{0.7} Pr^{0.4} \tag{31}$$

where

$$Nu_r = \psi^{-0.55}$$

$$\psi = 1 + \gamma(T_W - T_S)$$

and

$$\gamma = \left|\frac{1}{\rho}\frac{\partial \rho}{\partial T}\right|_P = \frac{1}{\rho}\frac{(\frac{\partial P}{\partial T})_\rho}{(\frac{\partial P}{\partial \rho})_T}$$

Properties for the above correlation are based on the coolant static temperature T_{CS}, and static pressure P_{CS}. Correlations described by equations (30) and (31) give inaccurate results when the coolant is liquid oxygen. A correlation, specifically for oxygen has been proposed [16]. This correlation is given by:

$$Nu = C_{C_n} Re_{CS} Pr^{0.4} \left(\frac{\overline{c_p}}{c_{pCS}}\right)^{2/3} \left(\frac{P_{Cri}}{P_{CS}}\right)^{0.2} \sqrt{\left(\frac{k_{CS}}{k_{CW}}\right)\left(\frac{\rho_{CW}}{\rho_{CS}}\right)} \tag{32}$$

where $P_{Cri} = 731.4$ psia is the critical pressure and

$$\overline{c_p} = \frac{i_{CW} - i_{CS}}{T_{CW} - T_{CS}}$$

The properties in the above correlations are calculated using the GASP program [3], or the WASP program [7] if the coolant is water. It should also be noted that there are three coolant heat transfer coefficients and adiabatic wall temperatures. They are for the top, side, and bottom walls of the cooling channel. The variable heat transfer coefficient is due to the variable wall temperature in the cooling channel. The coolant reference and adiabatic wall enthalpies are also functions of wall temperature and are larger for the surface nodes closer to the bottom of the cooling channel. The correlation factors for the heat transfer coefficient, C_{C_n}, in equations (30) and (31) are usually equal to 0.023 for most coolants. When the coolant is liquid oxygen, however, a factor of 0.0025 is used in equation (32).

The correlations given by equations (30)-(32) are for fully developed turbulent flow in a smooth and straight tube (channel). To include the effect of the entrance region, they are multiplied by the following coefficient [17]:

$$\phi_{Ent.} = 2.88 \left(\frac{\sum_{i=1}^{n} \Delta S_{i,i+1}}{d_{C_n}} \right)^{-0.325} \tag{33}$$

Other entrance effect factors for different types of cooling channel entrances reported in [17] are given by:

$$\phi_{Ent.} = \left[1 + \left(\frac{\sum_{i=1}^{n} \Delta S_{i,i+1}}{d_{C_n}} \right)^{-0.7} (T_w/T_b)^{0.1} \right] \tag{34}$$

for a 90^o bend entrance. Taylor [18] suggested the following correction factors:

$$\phi_{Ent.} = (T_W/T_b)^{[1.59/(\sum_{i=1}^{n} \Delta S_{i,i+1}/d_{C_n})]} \tag{35}$$

for straight tube and

$$\phi_{Ent.} = (T_W/T_b)^{[1.59/(\sum_{i=1}^{n} \Delta S_{i,i+1}/d_{C_n})]} \left[1 + 5/ \left(\frac{\sum_{i=1}^{n} \Delta S_{i,i+1}}{d_{C_n}} \right) \right] \tag{36}$$

for a 90^o bend entrance. The correction factor for the curvature effect is given by [19]:

$$\phi_{Cur.} = \left[Re_{CX_{Avg.}} \left(\frac{r_{C_n}}{R_{Cur._n}} \right)^2 \right]^{\pm 1/20} \tag{37}$$

where r_{C_n} is the hydraulic radius of cooling channel, $R_{Cur._n}$ is the radius of curvature, the sign (+) denotes the concave curvature and the sign (-) denotes the convex one. To incorporate the effect of surface roughness on the heat transfer coefficient, a simple empirical correlation is suggested by Norris [20]:

$$\frac{Nu}{Nu_{\text{smooth}}} = \left(\frac{f}{f_{\text{smooth}}} \right)^n \tag{38}$$

where $n = 0.68Pr^{0.215}$. For $f/f_{\text{smooth}} > 4.0$ Norris finds that the Nusselt number no longer increases with increasing roughness.

Once the heat transfer coefficients and adiabatic wall temperatures for the hot gas and coolant are evaluated, a finite difference model is used to re-evaluate the wall temperature distribution. This model has been specifically developed for three-dimensional conduction in a rocket thrust chamber and nozzle, as shown in Figure 1. Because of the symmetry of the configuration, computations are performed for only one cell (see Figure 3). Since no heat is

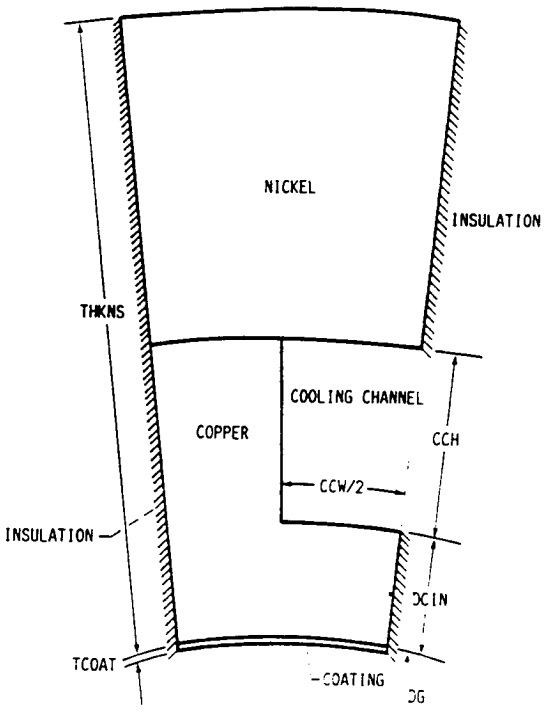

Figure 3. A Half Cooling Channel Cell.

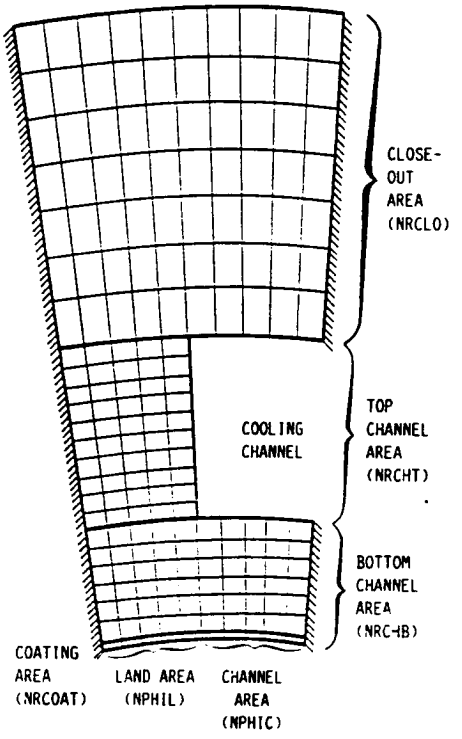

Figure 4. Finite Difference Grids Superimposed on Half of a Cooling Channel.

transferred to the two sides of the cell, they are assumed to be insulated. A finite difference grid is superimposed on the aforementioned cell as shown in Figure 4. In this program the number of nodes in the radial direction for different layers and in the circumferential direction for the land and channel area must be specified. Thus, the grid size can vary from one layer to another. Each node is connected to four neighboring nodes at the same station. It also exchanges heat with its counterpoints at two neighboring stations (i.e., stations $n+1$ and $n-1$). The finite difference equation for a node located in the middle of a material is given by

$$T^{l}_{i,j,n} = \frac{T^{l-1}_{i+1,j,n}/R_1 + T^{l-1}_{i,j-1,n}/R_2 + T^{l-1}_{i-1,j,n}/R_3 + T^{l-1}_{i,j+1,n}/R_4 + T_{i,j,n+1}/R_5 + T_{i,j,n-1}/R_6}{1/R_1 + 1/R_2 + 1/R_3 + 1/R_4 + 1/R_5 + 1/R_6} \tag{39}$$

where

$$R_1 = \frac{r\Delta\phi}{\Delta r\left(\Delta S^{n-1,n}_{i,j} + \Delta S^{n,n+1}_{i,j}\right)}\left(\frac{1}{k^{l-1}_{i,j,n}} + \frac{1}{k^{l-1}_{i+1,j,n}}\right)$$

$$R_2 = \frac{\Delta r}{(r+\frac{\Delta r}{2})\Delta\phi\left(\Delta S^{n-1,n}_{i,j} + \Delta S^{n,n+1}_{i,j}\right)}\left(\frac{1}{k^{l-1}_{i,j,n}} + \frac{1}{k^{l-1}_{i,j-1,n}}\right)$$

$$R_3 = \frac{r\Delta\phi}{\Delta r\left(\Delta S^{n-1,n}_{i,j} + \Delta S^{n,n+1}_{i,j}\right)}\left(\frac{1}{k^{l-1}_{i,j,n}} + \frac{1}{k^{l-1}_{i-1,j,n}}\right)$$

$$R_4 = \frac{\Delta r}{(r-\frac{\Delta r}{2})\Delta\phi\left(\Delta S^{n-1,n}_{i,j} + \Delta S^{n,n+1}_{i,j}\right)}\left(\frac{1}{k^{l-1}_{i,j,n}} + \frac{1}{k^{l-1}_{i,j+1,n}}\right)$$

$$R_5 = \frac{\Delta S^{n,n+1}_{i,j}}{2A_{i,j,n}}\left(\frac{1}{k^{l-1}_{i,j,n}} + \frac{1}{k_{i,j,n+1}}\right)$$

$$R_6 = \frac{\Delta S^{n-1,n}_{i,j}}{2A_{i,j,n-1}}\left(\frac{1}{k^{l-1}_{i,j,n}} + \frac{1}{k_{i,j,n-1}}\right)$$

$$A_{i,j,n} = \frac{(r\Delta\phi\Delta r)_{n+1} + (r\Delta\phi\Delta r)_n}{2}$$

and

$$A_{i,j,n-1} = \frac{(r\Delta\phi\Delta r)_n + (r\Delta\phi\Delta r)_{n-1}}{2}$$

and l is the Gauss-Siedel iteration index. Note that the above equation is a three-dimensional finite difference equation. The Gauss-Siedel iteration, however, is only performed for the nodes on the n-th station and $T_{i,j,n+1}$ and $T_{i,j,n-1}$ are kept constant during this iteration. The value of $T_{i,j,n-1}$ in equation (39) is from the recent march and $T_{i,j,n+1}$ from the previous march. The conductivity in equation (39) is a function of temperature, i.e., $k = k(T)$. Similar equations are derived for other nodes (boundary nodes and nodes at the interface between two

different materials). It should be noted that at the boundary nodes, depending on the boundary

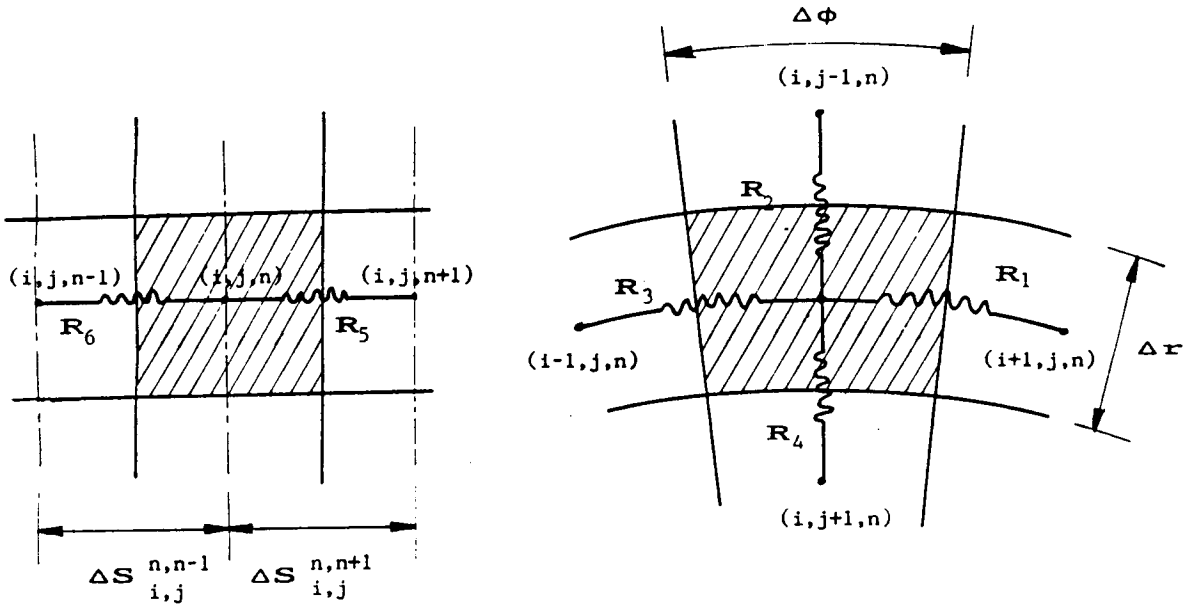

Figure 5. Resistances between a typical interior node and its adjoining nodes.

conditions, convective and radiative terms also appear in the nodal balance of energy equation. For example, for a node at the inner surface of the nozzle the finite difference equation is given by

$$T^{l}_{i,j,n} = \frac{T^{l-1}_{i+1,j,n}/R_1 + T^{l-1}_{i,j-1,n}/R_2 + T^{l-1}_{i-1,j,n}/R_3 + T_g/R_4 + T_{i,j,n+1}/R_5 + T_{i,j,n-1}/R_6 + Q_r}{1/R_1 + 1/R_2 + 1/R_3 + 1/R_4 + 1/R_5 + 1/R_6} \tag{40}$$

where

$$R_1 = \frac{2r\Delta\phi}{\Delta r\left(\Delta S^{n-1,n}_{i,j} + \Delta S^{n,n+1}_{i,j}\right)}\left(\frac{1}{k^{l-1}_{i,j,n}} + \frac{1}{k^{l-1}_{i+1,j,n}}\right)$$

$$R_2 = \frac{\Delta r}{(r+\frac{\Delta r}{2})\Delta\phi\left(\Delta S^{n-1,n}_{i,j} + \Delta S^{n,n+1}_{i,j}\right)}\left(\frac{1}{k^{l-1}_{i,j,n}} + \frac{1}{k^{l-1}_{i,j-1,n}}\right)$$

$$R_3 = \frac{2r\Delta\phi}{\Delta r\left(\Delta S^{n-1,n}_{i,j} + \Delta S^{n,n+1}_{i,j}\right)}\left(\frac{1}{k^{l-1}_{i,j,n}} + \frac{1}{k^{l-1}_{i-1,j,n}}\right)$$

$$R_4 = \frac{2}{h_g r\Delta\phi\left(\Delta S^{n-1,n}_{i,j} + \Delta S^{n,n+1}_{i,j}\right)}$$

$$R_5 = \frac{\Delta S^{n,n+1}_{i,j}}{2A_{i,j,n}}\left(\frac{1}{k^{l-1}_{i,j,n}} + \frac{1}{k_{i,j,n+1}}\right)$$

$$R_6 = \frac{\Delta S^{n-1,n}_{i,j}}{2A_{i,j,n-1}}\left(\frac{1}{k^{l-1}_{i,j,n}} + \frac{1}{k_{i,j,n-1}}\right)$$

$$A_{i,j,n} = \frac{\left[\left(r_0 + \frac{\Delta r}{4}\right)\Delta\phi\frac{\Delta r}{2}\right]_{n+1} + \left[\left(r_0 + \frac{\Delta r}{4}\right)\Delta\phi\frac{\Delta r}{2}\right]_{n}}{2}$$

$$A_{i,j,n-1} = \frac{\left[\left(r_0 + \frac{\Delta r}{4}\right)\Delta\phi\frac{\Delta r}{2}\right]_{n} + \left[\left(r_0 + \frac{\Delta r}{4}\right)\Delta\phi\frac{\Delta r}{2}\right]_{n-1}}{2}$$

Note that equation (40) is used when hot-gas-side heat transfer coefficient is known and wall heat flux is evaluated based on the temperature difference, i.e., equation (9). When wall heat flux (q_n) is known, equation (40) becomes

$$T^l_{i,j,n} = \Big[T^{l-1}_{i+1,j,n}/R_1 + T^{l-1}_{i,j-1,n}/R_2 + T^{l-1}_{i-1,j,n}/R_3 + T_{i,j,n+1}/R_5 + T_{i,j,n-1}/R_6 + q_n\Delta\phi(\Delta S^{n-1,n}_{i,j} + \Delta S^{n,n+1}_{i,j})/2 + Q_r\Big]/(1/R_1 + 1/R_2 + 1/R_3 + 1/R_5 + 1/R_6) \quad (41)$$

where q_n is wall heat flux which can be an input of the program or evaluated using equation (10). Q_r is the radiative heat transfer term which is evaluated based on the Discrete Exchange Factor (DEF) method [21, 22, 23, 24] and is given by:

$$Q_r = \frac{\Delta\phi(\Delta S^{n-1,n}_{i,j} + \Delta S^{n,n+1}_{i,j})sin\beta_n}{4\pi}\left(\sum_{l=1}^{m+2} w_{s_l}E_{s_l}\overline{DS_lS_n} + \sum_{l=1}^{m} w_{g_l}E_{g_l}\overline{DG_lS_n} - E_{s_n}\right) \quad (42)$$

E_{s_n} and E_{g_n} are surface and gas emissive powers at stations n and are related to their temperatures via

$$E_{s_n} = \epsilon\sigma\frac{2\pi r}{\sin\beta_n}T^4_{s_n}$$

$$E_{g_l} = 4K_{t_l}(1-\omega_0)\sigma\pi r^2 T^4_{g_l}$$

$\overline{DS_lS_n}$ and $\overline{DG_lS_n}$ are total exchange factors between differential surface and gas elements at station l to a surface element at station n. The total exchange factor between two elements is defined as the fraction of the radiative energy that is emitted from one element and is absorbed by the other element via direct radiation and multiple reflections and scatterings from surfaces and gas. Procedures for calculating direct and total exchange factors in rocket thrust chambers and nozzles are presented in [23] and [24]. The radiative heat transfer term, given by equation (42), evaluates the radiative energy coming to a surface node from all parts of the engine. This is done by numerical integration of the radiative energy incident on the surface at station n that is originated (emitted) from station l. The weight factors w_s and w_g are used for numerical integration of surface and gas radiation along axial direction. If the stations are equally spaced then the weight factors are the same as those of trapezoidal or Simpson methods. In the present application, however, the stations are more concentrated at the throat area and are unevenly spaced. The rectangular numerical integration method is suitable when stations are not equally spaced and the weight factors are equal to the width of each station, i.e., $(\Delta S^{n-1,n}_{i,j} + \Delta S^{n,n+1}_{i,j})/2$. It should be noted that the evaluation of exchange factors $\overline{DS_kS_n}$ and $\overline{DG_kS_n}$ involves multiple integration (see [23] and [24]) and requires significant computer time. Values of these exchange factors depend on the geometry of engine and radiative properties of combustion gases. Hence, they can be evaluated using external modules and the resulting

exchange factors stored in files for different engines. These files can then be used as inputs to the RTE. A separate computer program, namely RTE_DEF (Rocket Thermal Evaluation_Discrete Exchange Factor), has been developed for evaluation of the total exchange factors. Note that the combustion properties code given by Gordon and McBride [2] does not provide the radiative properties of combustion gases. These properties may be obtained from [25] and [26]. For example, if the fuel is RP-1, the combustion gas species mole fractions are obtained from the combustion code [5], containing 17%CO_2, 30%CO, 33%H_2O, 6%OH, 2.5%O_2, 3%H, 7%H_2 and 1.5%O. Using an integrated average value of the absorption coefficients of these species, the overall absorption coefficient is found to be $K_a = 2.5in^{-1}$.

Based on the revised wall temperature, new hot-gas and coolant wall properties, heat transfer coefficients and adiabatic wall temperatures are calculated using equations (1) through (42). Again, a new wall temperature distribution based on the most recent heat transfer coefficients and adiabatic wall temperatures is calculated using the finite difference subroutine for heat conduction within the wall. This procedure is repeated until the relative difference between the temperature distribution of two consecutive iterations becomes negligibly small. After the results for station n converge, the coolant Mach number and entropy as functions of static pressure and enthalpy ($M_{C_n}, s_{C_n} = f(P_{CS_n}, i_{CS_n})$) are evaluated using the GASP or WASP programs. Next, the coolant stagnation pressure is evaluated based on the coolant entropy and stagnation enthalpy, i.e., $P_{C0_n} = P(i_{C0_n}, s_{C_n})$. The GASP and WASP programs do not have explicit expressions for pressure in terms of entropy and enthalpy. Thus, an implicit relation for stagnation pressure (i.e., $s_{C_n} = s(P_{C0_n}, i_{C_n})$) with the secant method for solving nonlinear equations is used to determine P_{C0_n}. In the secant method, two initial guesses for the stagnation pressures were made ($P_1 = P_{C0_{n-1}} + 20$ and $P_2 = P_{C0_{n-1}} - 20$) and the corresponding entropies s_1 and s_2 were determined. The secant method's iterative equation is given by:

$$P_{k+1} = P_k - s_k \frac{P_{k-1} - P_k}{s_{k-1} - s_k} \tag{43}$$

where k is the iteration index. When equation (43) converges (the convergence criterion is $|s_k - s_{C_n}| < 0.0001$), the coolant stagnation is set equal to the latest value of P_k. Finally, the coolant stagnation temperature is determined based on the coolant stagnation pressure and enthalpy ($T_{C0_n} = T(P_{C0_n}, i_{C0_n})$).

The program then marches axially and performs similar calculations (i.e., equations (1) through (43)) for all stations. Once the results of the last station (station m) converged, the results of this march are compared to those of the previous march. If the relative differences between the results of two consecutive marches is less than the axial convergence criterion the program stops, otherwise it continues its axial marches until convergence is achieved. The effect of axial conduction can be eliminated by setting the axial convergence criterion greater than one or setting the maximum number of passes equal to one. A complete flow chart of RTE is presented in [1].

The method described here, i.e., axial marches along axial direction, has several advantages over the direct solution of a three-dimensional finite difference formulation. First, it converges very quickly. Second, it requires less memory. Third, it allows the user to control the importance of axial conduction by allowing for different convergence criterion between the axial and radial and circumferential directions. For example, in analysis of a thin-walled, radiatively-cooled, low-pressure engine, axial conduction is negligible. In this case one might set the convergence accuracy to 5% in the axial direction and 0.1% in the other directions. In

the case of a thick-walled, regeneratively-cooled, high-pressure engine, axial conduction may be significant. Thus, the accuracy in the axial direction may be set to 0.1% and 0.1% in the other directions.

Results of a Typical Run

RTE is used to determine the temperature distribution and heat transfer characteristics of a Liquid Oxygen/ Liquid Hydrogen rocket engine. The engine has the following specifications:

Fuel	LH_2
Oxidant	LO_2
Coolant	LH_2
Chamber stagnation pressure P_{GO}	1600 psi
Coolant stagnation pressure P_{CO}	2400 psi
Fuel flow rate	35.412 lb/sec
Coolant flow rate	5.059 lb/sec
Fuel/Oxidant Mixture ratio	5.9957
Coolant stagnation temperature	110 R
Number of cooling channels	100

The engine is subdivided into 29 stations. Table 1 shows dimensions of the engine and some thermal characteristics at each station (see Figure 3 for notation). Note that dimensions given in Table 1 are in inches. Also, $DCIN = 0.035$ in. remains constant along the engine. The outer surface radiates to space and its emissivity is 0.9. The thermal conductivities of wall materials, i.e., nickel and copper are functions of temperature.

The resulting wall temperature distributions for stations 1, 9, 16 and 29 are shown in Figure 6. A close examination of the temperature distributions reveals that the temperature gradient is relatively large in radial direction , especially for station 9. This may also be true for any other high pressure thrust chamber. Also, the results shown in Figure 6 can be used to optimize the cooling channel aspect ratio. For example, there is no temperature gradient at the upper section of the cooling channel in Figure 6a (station 9, throat). Hence, the cooling channel can be shorten slightly without changing the overall heat transfer to the coolant.

HOT-GAS-SIDE BOUNDARY LAYER ANALYSIS INTERFACE

The convective heat transfer coefficients and heat fluxes for the hot-gas-side of the RTE are evaluated based on a tube-like correlation [8], see equation (7). To obtain more accurate results, RTE can be linked to a nozzle flow and boundary layer analysis program. The procedure for linking RTE to TDK (Two-Dimensional Kinetics Nozzle Performance Computer Program [5]) is described in this section. A similar approach may be implemented to link RTE to other nozzle boundary layer analysis programs.

The flowchart for the iterative procedure for linking RTE to TDK is shown in Figure 7. In this approach, initially, the wall fluxes and temperatures are evaluated by running RTE under an unknown wall heat flux condition. In this run, RTE uses it internal hot-gas-side routines. The wall temperatures calculated by RTE are then used in the inputs of TDK. Using one of TDK's boundary layer modules (BLM or MABL)[5], a new wall heat flux distribution is

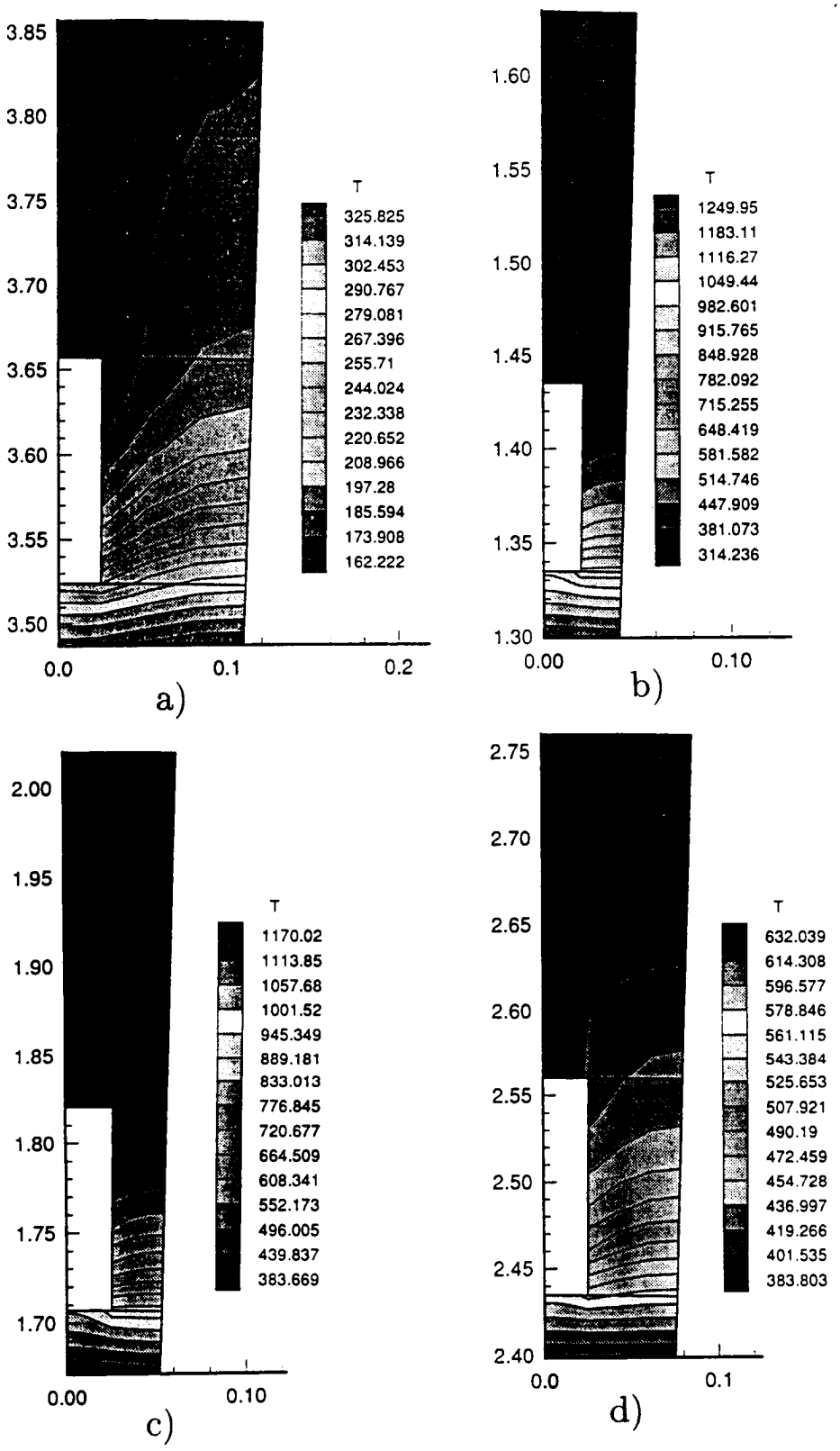

Figure 6. Temperature distribution at stations a) 1, b) 9, c) 16 and d) 29.

evaluated. The wall heat flux distribution is inserted into the RTE inputs. This time, since the hot-gas-side heat fluxes are known, RTE bypasses all hot-gas-side calculations (e.g., its CET subroutine and hot-gas-side heat transfer coefficient correlations) and calculates the wall temperature distribution. The new wall temperature distribution along the axial direction is then input to TDK and a new heat flux distribution is calculated. This iterative procedure continues until convergence is reached.

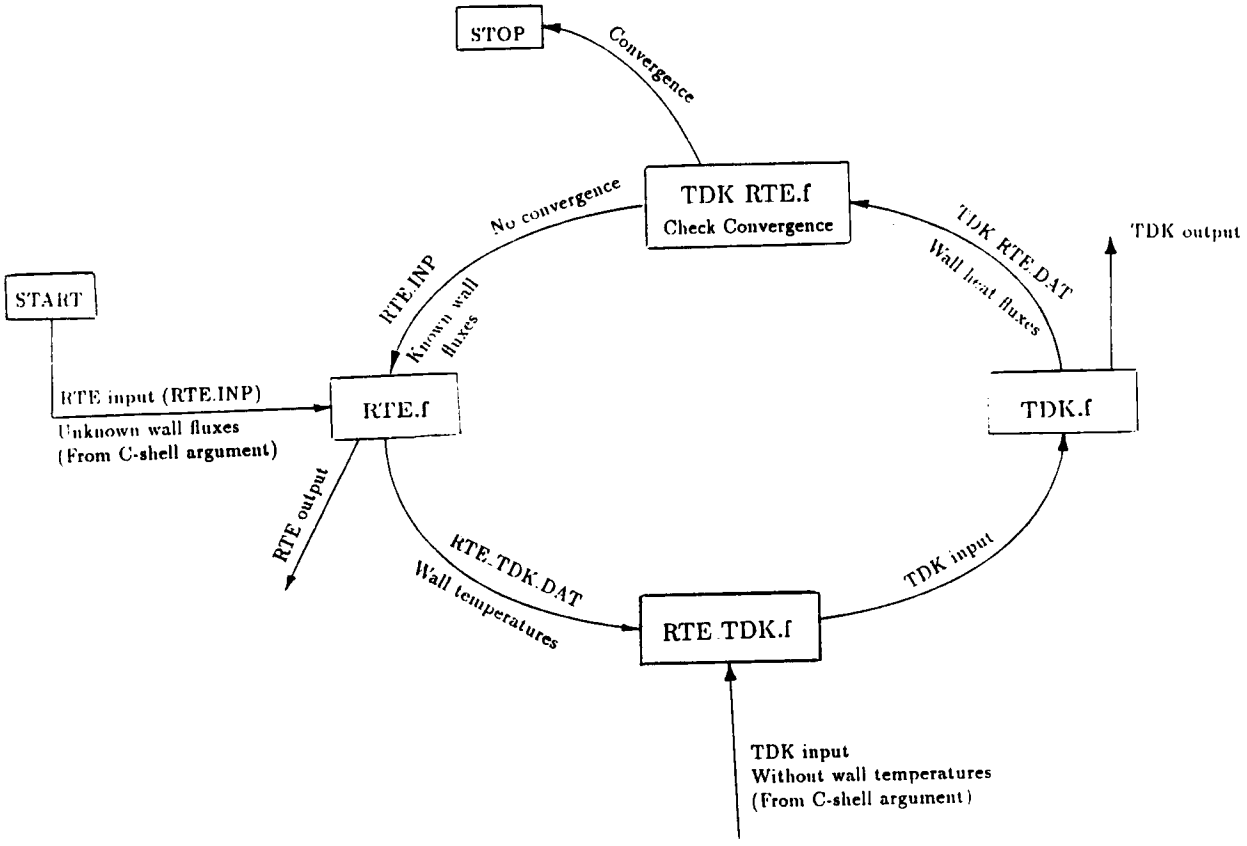

Figure 7. Flowchart of RTE-TDK Interface.

The RTE-TDK model is used to predict wall heat fluxes and temperatures of the LO/LH engine presented in the previous section. The resulting wall heat flux and temperature distributions for both RTE and RTE-TDK calculations are shown in Figures 8 and 9. As shown in these figures, the heat flux and temperature distribution when the boundary layer module is used are consistently below those calculated via hot-gas-side heat transfer coefficient, i.e., equation (5). The reduction of heat flux and temperature is due to the relaminarization of accelerating flow.

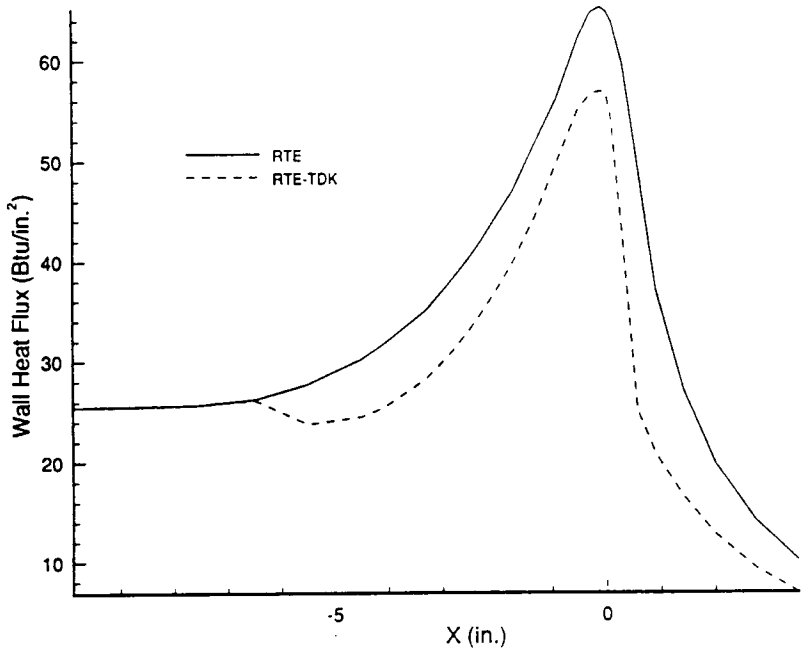

Figure 8. Wall heat fluxes for a H2 cooled engine based on RTE and RTE-TDK models.

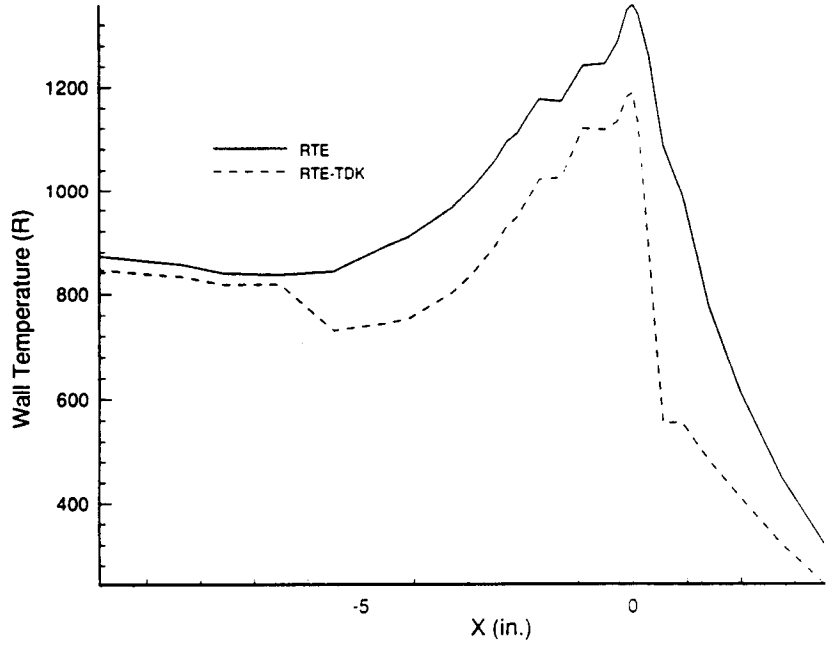

Figure 9. Wall temperatures for a H2 cooled engine based on RTE and RTE-TDK models.

Table 1: Parameters of thrust chamber and nozzle at different stations.

Station	X	DG	CCW	CCH	$THKNS$
1	3.55	6.978	0.05	0.133	0.368
2	2.75	5.898	0.05	0.123	0.358
3	2.0	4.886	0.05	0.113	0.348
4	1.4	4.076	0.05	0.104	0.339
5	0.9	3.402	0.05	0.1	0.335
6	0.559	2.942	0.04	0.1	0.335
7	0.3	2.692	0.04	0.1	0.335
8	0.1	2.610	0.04	0.1	0.335
9	0.	2.6	0.04	0.1	0.335
10	-0.1	2.608	0.04	0.1	0.335
11	-0.274	2.656	0.04	0.1	0.335
12	-0.506	2.746	0.04	0.1	0.335
13	-0.906	3.924	0.05	0.1	0.335
14	-1.306	3.092	0.05	0.1	0.335
15	-1.706	3.264	0.05	0.104	0.339
16	-1.906	3.344	0.05	0.113	0.348
17	-2.106	3.432	0.05	0.123	0.358
18	-2.306	3.516	0.05	0.125	0.36
19	-2.506	3.602	0.05	0.125	0.36
20	-2.906	3.77	0.05	0.125	0.36
21	-3.306	3.94	0.05	0.125	0.36
22	-4.106	4.236	0.05	0.125	0.36
23	-4.506	4.358	0.05	0.125	0.36
24	-5.506	4.6	0.05	0.125	0.36
25	-6.506	4.744	0.05	0.125	0.36
26	-7.572	4.8	0.05	0.125	0.36
27	-8.35	4.8	0.05	0.125	0.36
28	-9.0	4.8	0.05	0.125	0.36
29	-9.875	4.8	0.05	0.125	0.36

CONCLUDING REMARKS

The numerical model for a rocket thermal analysis code (RTE) has been discussed. This model allows temperature variation along three directions: axial, radial and circumferential. The numerical results presented show that there is a large temperature gradient in the axial direction for engines with a high chamber pressure. The resulting wall temperature distribution can be used to optimize the cooling channel aspect ratios

The RTE needs to be modified further to incorporate a wide range of cooling channel shapes and a CFD model for the cooling channel flow analysis. Efforts are presently under way to include these items in the RTE.

Acknowledgment

RTE has been developed as a result of collaborative efforts between the author and NASA Lewis Research Center. The author wishes to thank his NASA colleagues, James Giuliani,

Michael Meyer, Harold Price, Richard Quentmeyer, Elizabeth Roncace and Mary Wadel for their suggestion and helps during development of RTE.

NOMENCLATURE

A	area
C	correlation factor for heat transfer coefficient
C_p	specific heat
d	diameter
$\overline{DG_kS_n}$	total exchange factor between gas and surface differential elements
$\overline{DS_kS_n}$	total exchange factor between two surface differential elements
e	cooling channel surface roughness
E	surface and gas emissive power
f	friction factor
g_c	gravitational constant, 32.2 ft.$lb_m/lb_f.s^2$
h	heat transfer coefficient
i	enthalpy
J	work/heat proportionality factor
k	conductivity
K_t	total extinction coefficient
m	total number of axial stations
N	total number of cooling channels
P	pressure
Pr	Prandtl number
q	heat flux
Q_r	radiative heat transfer at inner surface
r	radius
$R_{Cur.}$	radius of curvature
R_n	thermal resistance
Re	Reynolds number
s	entropy
T	temperature
V	velocity
W	weight flow
w	weight factor for discrete exchange factor method
x	station position in longitudinal direction

Greek Symbols

β	angle between a vector normal to the nozzle surface and axial direction
ΔS	length of cooling channel between two stations
Δp	pressure drop
Δr	radial mesh size
$\Delta\phi$	circumferential mesh size
ϵ	convergence criteria or error limit
μ	dynamic viscosity

ρ	density
σ	Stefan-Boltzmann coefficient
ϕ	entrance and curvature effect correction factors

Subscripts

A	adiabatic
$Avg.$	average
C	coolant
$Cur.$	curvature
f	viscous or friction
G	gas
i	node i
j	node j
k	secant method iteration number
M	momentum
n	related to station n
r	radiation
S	static
s	surface
W	wall
X	reference
0	stagnation

Superscripts

j	iteration number
l	iteration number for conduction model
n	related to station n

References

[1] Naraghi, M.H.N., RTE - A Computer Code for Three-Dimensional Rocket Thermal Evaluation, Revision 2, Manhattan College Report for NASA Lewis Research Center, Grant NAG 3-892, July 1991.

[2] Gordon, S. and McBride, B. J., "Computer Program for Calculation of complex Chemical Equilibrium Compositions, Rocket Performance, Incident and Reflection Shocks, and Chapman-Jouquet Detonations," NASA SP-270, 1971.

[3] Hendricks, R. C., Baron, A. K. and Peller, I. C., "GASP - A Computer Code for Calculating the Thermodynamic and Transport Properties for Ten Fluids: Parahydrogen, Helium, Neon, Methane, Nitrogen, Carbon Monoxide, Oxygen, Fluorine, Argon, and Carbon Dioxide," NASA TN D-7808, Feb. 1975.

[4] Muss, J.A., Nguyen, T.V., and Johnson, C.W., "User's Manual for Rocket Combustor Interactive Design (ROCCID) and Analysis Compter Program," Volumes I and II, NASA Contractor Report 1087109, May 1991.

[5] Nickerson, G.R., Coats, D.E., Dang, A.L., Dunn, S.S., and Kehtarnavaz, H., "Two-Dimensional Kinetics (TDK) Nozzle Performance Computer Program," NAS8-36863, March 1989.

[6] Gordon, S., McBride, B. J. and Zeleznik, F. J., "Computer Program for Calculation of Complex Chemical Equilibrium Compositions and Applications Supplement I - Transport Properties," NASA TM-86885, Oct. 1984.

[7] Hendricks, R. C., Peller, I. C. and Baron, A. K., "WASP - A Flexible Fortran IV Computer Code for Calculating Water and Steam Properties," NASA TN D-7391, Nov. 1973.

[8] Eckert, E. R. G. and Drake, R. M., "Analysis of Heat and Mass Transfer," McGraw-Hill Book Company, 1972.

[9] Bartz, D. R., "Turbulent Boundary-Layer Heat Transfer from Rapidly Accelerating Flow of Rocket Combustion Gases and of Heated Air," Advances in Heat Transfer, pp. 2-108, 1965.

[10] Colebrook, C.F., "Turbulent Flow in Pipes with Particular Reference to the Transition Region Between the Smooth and Rough Pipe Laws," Journal of Institute of Civil Engineers, Vol. 11, pp. 133-156, 1939.

[11] Chen, N.H., "An Explicit Equation for Friction Factor in Pipe," Ind. Eng. Chem. Fundam., Vol. 18, No. 3, pp. 296-297, 1979.

[12] Itō, H., "Friction Factors for Turbulent Flow in Curved Pipes," Journal of Basic Engineering, pp. 123-134, 1959.

[13] Moody, L.F., "Friction Factors for Pipe Flow," Transactions of ASME, pp. 671-684, 1944.

[14] Hendricks, R. C., Niino, M., Kumakawa, A., Yernshenko, V. M., Yaski, L. A., Majumdar, L. A., and Mukerjee, J., "Friction Factors and Heat Transfer Coefficients for Hydrogen Systems Operating at Supercritical Pressures," Proceeding of Beijing International Symposium on Hydrogen Systems, Beijing, China, May 7-11, 1985.

[15] Kumakawa, A., Niino, M., Hendricks, R.C., Giarratano, P.J. and Arp, V.D., "Volume-Energy Parameters for Heat Transfer to Supercritical Fluids," Proceeding of the Fifteenth International Symposium of Space Technology and Science, Tokyo, pp. 389-399, 1986.

[16] Spencer, R.G. and Rousar, D.C., "Supercritical Oxygen Heat Transfer," NASA CR-135339, 1977.

[17] Niino, M., Kumakawa, A., Yatsuyanagi, N. and Suzuki, A., "Heat Transfer Characteristics of Liquid Hydrogen as a Coolant for the LO2/LH2 Rocket thrust Chamber with the Channel Wall Construction," 18Th. AIAA/SAE/ASME Joint Propulsion Conference, Cheveland, Ohio, June 21-23, 1982, AIAA paper 82-1107.

[18] Taylor, M.F.,"A Method of Predicting Heat Transfer Coefficients in the Cooling Passages of Nerva and Phoebus-2 Rocket Nozzles," NASA TM X-52437, June 1968.

[19] Owhadi, A., Bell, K.J. and Crain, B., "Forced Convection Boiling Inside Helically-Coiled Tubes," International Journal of Heat and Mass Transfer, Vol. 11. pp. 1779-1793. 1968.

[20] Norris, R.H., "Augmentation of Convection Heat and Mass Transfer." American Society of Mechanical Engineers, New York, 1971.

[21] Naraghi, M.H.N., Chung, B.T.F., and Litkouhi, B., "A Continuous Exchange Factor Method for Radiative Analysis of Enclosures with Participating Media," Journal of Heat Transfer, Trans. ASME, Vol. 110, pp. 456-462, 1988.

[22] Naraghi, M.H.N., and Kassemi, M., "Radiative Heat Transfer in Rectangular Enclosures: A Discrete Exchange Factor Solution," Journal of Heat Transfer, Trans. ASME, Vol. 111, pp. 1117-1119, 1989.

[23] Hammad, K.J., and Naraghi, M.H.N., "Exchange Factor Model for Radiative Heat Transfer Analysis in Rocket Engines," AIAA Journal of Thermophysics and Heat Transfer, Vol. 5, No. 3, pp. 327-334, 1991.

[24] Hammad, K.J., "Radiative Heat Transfer in Rocket Thrust Chambers and Nozzles," M.S. Thesis, Department of Mechanical Engineering, Manhattan College, 1989.

[25] Ludwig, C.B., Malkmus, W., Reardon, J.E., and Thomson, J.A.L., "Handbook of Infrared Radiation From Combustion Gases," NASA SP-3080, 1973.

[26] Siegel, R., and Howell, J.R., Thermal Radiation Heat Transfer, Hemisphere Publishing Corporation, 3rd Ed., 1992.